OTFS-Modulated MIMO Faster-than-Nyquist Signaling in Doubly Selective Fading Channel

Zekun Hong and Shinya Sugiura*
Institute of Industrial Science, The University of Tokyo
E-mail: {zekunhong@g.ecc.u-tokyo.ac.jp, sugiura@iis.u-tokyo.ac.jp}

***Abstract*—This paper proposes a novel reduced-complexity detection scheme for multiple-input multiple-output (MIMO)-assisted faster-than-Nyquist (FTN) signaling scheme in the doubly selective fading channels. By utilizing the channel's sparse approximation, we exploit a simplified linear minimum mean square error (LMMSE) algorithm with a log-linear complexity. The proposed scheme attains the same bit error rate performance as the conventional LMMSE detector while attaining a significantly lower complexity. Furthermore, we propose the amalgamation of MIMO-FTN signaling and orthogonal time frequency space modulation and conceive the low-complexity delay Doppler domain detection algorithm by exploiting the channel's sparsity.**

I. Introduction

Faster-than-Nyquist (FTN) signaling [1] is a technique that constitutes a shorter symbol interval than that defined by the classic Nyquist criterion, which is free from intersymbol interference (ISI). From the information-theoretic perspective, the benefits of FTN signaling are attained from the excess bandwidth that cannot be exploited in the Nyquist-based signaling scheme employing realistic pulse shaping [1]. To reduce the complexity imposed by the FTN-specific ISI effects, several time-domain (TD) [2], frequency-domain (FD) [3, 4], and message-passing (MP)-based [5] demodulation schemes were proposed. Moreover, precoded FTN signaling schemes based on matrix factorization were proposed [6–9]. Kim [6] used eigenvalue decomposition (EVD) of an FTN-specific ISI matrix for precoding at the transmitter and weighting at the receiver. In [8], EVD-precoded FTN signaling with optimal power allocation was developed, and the system parameters were optimized to maximize mutual information in frequency-flat and frequency-selective fading channel. In [9], fast Fourier transform (FFT)-spread multi-carrier FTN (MFTN) signaling was proposed to reduce the computational complexity imposed by EVD-based diagonalization for the frequency-selective fading channel [8].

Several FTN signaling schemes were designed for the doubly selective fading channel to improve robustness to the Doppler shift and delay spread [10–12]. Wu *et al.* [10] proposed the Gaussian MP (GMP) detector, which is assisted by a vector form factor graph. In [11], EVD-precoded FTN signaling was designed for an underwater acoustic doubly selective channel. In [12], differential multi-carrier FTN signaling was proposed, which approximately diagonalizes the FTN-specific ISI matrix as well as the noise correlation matrix and dispenses with any channel sate information (CSI).

In addition to the above-mentioned single-input single-output (SISO) FTN signaling systems, employing FTN signaling in multiple-input multiple-output (MIMO) systems is a promising direction to further enhance spectral efficiency and data throughput. In [13], the Mazo limit associated with the MIMO system was analyzed, while in [14–16], the capacity of MIMO-FTN signaling was studied. In [17], inter-carrier interference (ICI) cancellation was discussed for MIMO-FTN signaling in a bandwidth-limited optical transmission system, while in [18], performance evaluation was conducted for MIMO-FTN signaling in the frequency-selective fading channel with the full-complexity minimum mean-square error (MMSE) equalizer. A low-complexity linear precoding and equalization method was conceived for MIMO-FTN covert communication in the additive white Gaussian noise (AWGN) channel [19]. To the best of our knowledge, most previous low-complexity FTN signaling receivers have been designed mainly for the SISO systems rather than the MIMO counterparts.

Most recently, two studies considered combining FTN signaling and orthogonal time frequency space (OTFS) modulation [20, 21], which exploits the sparsity and quasi-static channel representation in the delay-Doppler (DD) domain. In [20], the OTFS-modulated FTN (OTFS-FTN) signaling was proposed based on full-complexity EVD-based precoding and detection. In [21], the integrated sensing and communications (ISAC) waveform was designed based on the fusion of OTFS and FTN signaling while assuming the use of an ideal bi-orthogonality pulse-shaping filter. Note that the above-mentioned OTFS-FTN signaling schemes are only investigated in single-antenna scenarios.

Against this background, the novel contributions of this paper are as follows. We propose a reduced-complexity detection scheme for MIMO-FTN signaling in the doubly selective fading channel. Our detection algorithm is designed for exploiting sparse approximation of the FTN-specific channel matrix, as well as efficient sparsity-assisted linear MMSE (LMMSE) equalization. We derive the theoretical achievable information

Preprint for publication in *IEEE International Conference on Communications (ICC) Workshop*, Montreal, Canada, 2025, DOI: 10.1109/ICCWorkshops67674.2025.11162265. © 2025 IEEE. Personal use of this material is permitted. Permission from IEEE must be obtained for all other uses, in any current or future media, including reprinting/republishing this material for advertising or promotional purposes, creating new collective works, for resale or redistribution to servers or lists, or reuse of any copyrighted component of this work in other works.

rate of the proposed MIMO-FTN signaling scheme. Finally, to further enhance the achievable performance against the high Doppler shift, we conceive for the first time the amalgamation of MIMO-FTN signaling and OTFS modulation. We derive the input-output relationship for the MIMO-OTFS-FTN signal and propose the reduced-complexity detection scheme, operated in the DD domain.[1]

II. System Model

Consider a MIMO-FTN signaling system supporting N_t transmit antennas and N_r receive antennas. The symbols transmitted from the the v-th antenna ($1 \leq v \leq N_t$) are represented by $\mathbf{x}_v = [x_{v,0}, \cdots, x_{v,N-1}]^T \in \mathbb{C}^N$, where N is the block length. The average symbol energy is given by $\mathbb{E}[|x_{v,n}|^2] = \sigma_s^2 (n = 0, \cdots, N-1)$. In order to avoid the detrimental effects of inter-block interference (IBI) caused by FTN signaling as well as the delay spread, the $2c$-length cyclic prefix (CP) symbols are added to the end of $\mathbf{x}_v$ as follows:

$$\begin{aligned}\mathbf{x}_v^{\mathrm{cp}} &= \left[x_{v,0}^{\mathrm{cp}}, \ldots, x_{v,N+2c-1}^{\mathrm{cp}}\right]^T \in \mathbb{C}^{N+2c} \\ &= [x_{v,0}, \ldots, x_{v,N-1}, x_{v,0}, \ldots, x_{v,2c-1}]^T \\ &= \mathbf{A}_{\mathrm{cp}} \mathbf{x}_v, \end{aligned} \tag{1}$$

where we have the CP-added matrix of

$$\mathbf{A}_{\mathrm{cp}} = \begin{bmatrix} \mathbf{I}_N & \\ \mathbf{I}_{2c} & \mathbf{0}_{2c\times(N-2c)} \end{bmatrix} \in \mathbb{R}^{(N+2c)\times N}. \tag{2}$$

Then, $\mathbf{x}_v^{\mathrm{cp}}$ is passed through a root-raised-cosine (RRC) pulse-shaping filter $h(t)$ with the roll-off factor β, to generate the baseband time-domain FTN signal as $x_v(t) = \sum_{n=0}^{N+2c-1} x_{v,n}^{\mathrm{cp}} h(t - nT)$, where we have the FTN symbol interval $T = \alpha T_0$. The FTN symbol's packing ratio α, and the Nyquist-criterion-based symbol interval $T_0 = 1/(2W)$, while $2W$ corresponds to the bandwidth of an ideal rectangular pulse filter. Note that adding a sufficiently long CP eliminates the effects of IBI induced by FTN signaling and the delay spread. Moreover, in this paper, we consider the practical range of the packing ratio, i.e., $\alpha \geq 1/(1+\beta)$ [9, 12].

We assume an L-tap frequency-selective fading channel of each pair between the transmit and receive antenna elements. After matched filtering by $h^*(-t)$, the received signal at the u-th receive antenna is expressed by

$$y_u(t) = \sum_{v=1}^{N_t} \sum_{n=0}^{N+2c-1} \sum_{i=0}^{L-1} h_{uv,i} x_{v,n}^{\mathrm{cp}} g(t-(i+n)T) + \eta_u(t), \tag{3}$$

where $h_{uv,i} \in \mathbb{C}$ is the channel coefficient between the v-th transmit to the u-th receive antennas for the i-th tap. Moreover, $g(t) \triangleq h(t) * h^*(-t)$ corresponds to the time response of the raised-cosine (RC) filter, $\eta_u(t) \triangleq n_u(t) * h^*(-t)$ is the FTN-specific correlated noise, and $n_u(t)$ represents the zero-mean complex-valued AWGN component at the u-th receive antenna. Also, the power spectral density of the AWGN is given by σ_0^2. Furthermore, the noise autocorrelation is calculated as $\mathbb{E}[\eta_u(nT)\eta_u^*(mT)] = \sigma_0^2 g((n-m)T)$.

By sampling $y_u(t)$ with the FTN interval T and removing the first c and last c samples in each frame, the received samples at the u-th receive antenna are given by

$$\begin{aligned}\mathbf{y}_u &= [y_{u,0}, \cdots, y_{u,N-1}]^T \in \mathbb{C}^N \\ &= \sum_{v=1}^{N_t} \mathbf{R}_{\mathrm{cp}} \widetilde{\mathbf{H}}_{u,v} \mathbf{A}_{\mathrm{cp}} \mathbf{x}_v + \boldsymbol{\eta}_u, \end{aligned} \tag{4}$$

where $\mathbf{R}_{\mathrm{cp}} = \begin{bmatrix} \mathbf{0}_{N\times c} & \mathbf{I}_N & \mathbf{0}_{N\times c} \end{bmatrix} \in \mathbb{R}^{N\times(N+2c)}$. The covariance matrix of $\boldsymbol{\eta}_u \in \mathbb{C}^N$ can be denoted as $\mathbb{E}\left[\boldsymbol{\eta}_u \boldsymbol{\eta}_u^H\right] = \sigma_0^2 \mathbf{G}$, where $\mathbf{G} \in \mathbb{R}^{N\times N}$ is a Toeplitz matrix, whose first row is denoted by $[g(0), g(-T) \cdots, g(-(N-1)T)]$. Furthermore, $\widetilde{\mathbf{H}}_{u,v} \in \mathbb{C}^{(N+2c)\times(N+2c)}$ denotes the effective channel matrix between the v-th transmit antenna to the u-th receive antenna. More specifically, the kth-row and mth-column entry of $\widetilde{\mathbf{H}}_{u,v}$ is given by

$$\widetilde{\mathbf{H}}_{u,v}[k,m] = \sum_{i=0}^{L-1} h_{uv,i} g(kT - (m+i)T). \tag{5}$$

The input-output relationship of the MIMO-FTN signaling system can be expressed as

$$\mathbf{y} = \mathbf{H}\mathbf{x} + \boldsymbol{\eta}, \tag{6}$$

where $\mathbf{y} = [\mathbf{y}_1^T, \cdots, \mathbf{y}_{N_r}^T]^T \in \mathbb{C}^{NN_r}$, $\mathbf{x} = [\mathbf{x}_1^T, \cdots, \mathbf{x}_{N_t}^T]^T \in \mathbb{C}^{NN_t}$, and $\boldsymbol{\eta} = [\boldsymbol{\eta}_1^T, \cdots, \boldsymbol{\eta}_{N_r}^T]^T \in \mathbb{C}^{NN_r}$. Assuming that the noise samples from different receiving antennas are independent of each other, i.e., $\mathbb{E}[\eta_u(nT)\eta_v^*(mT)] = 0, u \neq v, \forall n, m \in \mathbb{R}$, we can obtain the covariance matrix of $\boldsymbol{\eta}$ as $\mathbb{E}\left[\boldsymbol{\eta}\boldsymbol{\eta}^H\right] = \sigma_0^2 \mathbf{G}_{\mathrm{r}} \in \mathbb{R}^{NN_r\times NN_r}$, where $\mathbf{G}_{\mathrm{r}} = \mathbf{I}_{N_r} \otimes \mathbf{G}$. Furthermore, the channel matrix $\mathbf{H} \in \mathbb{C}^{NN_r\times NN_t}$ is expressed as

$$\mathbf{H} = \begin{bmatrix} \mathbf{H}_{1,1} & \cdots & \mathbf{H}_{1,N_t} \\ \vdots & \ddots & \vdots \\ \mathbf{H}_{N_r,1} & \cdots & \mathbf{H}_{N_r,N_t} \end{bmatrix}, \tag{7}$$

where $\mathbf{H}_{u,v} = \mathbf{R}_{\mathrm{cp}} \widetilde{\mathbf{H}}_{u,v} \mathbf{A}_{\mathrm{cp}}$.

III. Reduced-Complexity MIMO-FTN Signaling Receiver Under Doubly Selective Fading Channel

A. Reduced-Complexity Diagonalization and Equalization

In the time-varying channel, the k-th received sample at the u-th receive antenna in (3) is rewritten by

$$\begin{aligned} y_u(kT) = &\sum_{v=1}^{N_t} \sum_{n=0}^{N+2c-1} \sum_{i=0}^{L-1} h_{uv,i,k} x_{v,n}^{\mathrm{cp}} g((k-i-n)T) \\ &+ \eta_u(kT), \end{aligned}$$

where $h_{uv,i,k}$ is the channel coefficient of the i-th tap at symbol index k between the v-th transmit antenna and the u-th receive antenna. The correlation between the channel coefficients $h_{uv,i,k}$ and $h_{uv,i,k+m}$ is defined as $\mathbb{E}[h_{uv,i,k} h_{uv,i,k+m}^*] = J_0(2\pi m \alpha F_d T_0)$ [8, 12], where $J_0(\cdot)$ denotes the zero-order

[1] *Notations*: $\mathbf{I}_N$ denotes the $N \times N$ identity matrix. $\mathbf{0}_{N\times M}$ denotes the $N \times M$ zero matrix. $\mathbf{F}_N$ represents the N-point normalized discrete Fourier transform (DFT) matrices. More specifically, the kth-row and lth-column entry of $\mathbf{F}_N$ is given by $(1/\sqrt{N}) e^{-2\pi j(k-1)(l-1)/N}$.

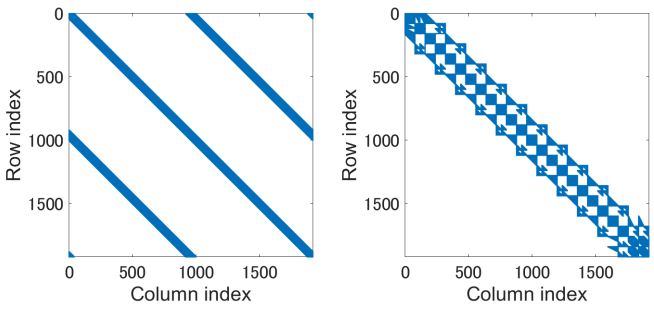

Fig. 1. (a) The matrix structure of $\mathbf{H}_{\mathrm{s}}\mathbf{H}_{\mathrm{s}}^H+\sigma_0^2\widetilde{\mathbf{G}}_{\mathrm{c}}$. (b) The reordered matrix.

Bessel function of the first kind, F_d denotes the maximum Doppler shift, and F_dT_0 denotes the normalized Doppler frequency. Hence, $\widetilde{\mathbf{H}}_{u,v}[k,m]$ in (5) is replaced by $\widetilde{\mathbf{H}}_{u,v}[k,m]=\sum_{i=0}^{L-1}h_{uv,i,k}g(kT-(m+i)T)$.

Based on (6), the LMMSE equalization considering noise whitening is given by

$$\hat{\mathbf{s}}_{\mathrm{MMSE}}=\mathbf{H}^H\left(\mathbf{H}\mathbf{H}^H+\sigma_0^2\mathbf{G}_{\mathrm{r}}\right)^{-1}\mathbf{y}. \tag{8}$$

We consider a sparse matrix approximation of $\hat{\mathbf{H}}_{\mathrm{u,v}}\approx\mathbf{R}_{\mathrm{cp}}\widetilde{\mathbf{H}}_{u,v}\mathbf{A}_{\mathrm{cp}}$. More specifically, the k-th row of $\hat{\mathbf{H}}_{\mathrm{u,v}}$ is given by

$$\Bigg[\underbrace{0,\ldots,0}_{k-1},\sum_{i=0}^{L-1}h_{uv,i,k+c}g((-c+i)T),\ldots,\sum_{i=0}^{L-1}h_{uv,i,k+c}g((c+i)T),\underbrace{0,\ldots,0}_{N-2c-k}\Bigg]\quad\text{for } k\le N-2c, \tag{9}$$

and

$$\Bigg[\sum_{i=0}^{L-1}h_{uv,i,k+c}g((N-c-k+i+1)T),\ldots,\sum_{i=0}^{L-1}h_{uv,i,k+c}g((c+i)T),\underbrace{0,\ldots,0}_{N-2c-1},\sum_{i=0}^{L-1}h_{uv,i,k+c}g((-c+i)T),\ldots,\sum_{i=0}^{L-1}h_{uv,i,k+c}g((N-c-k+i)T)\Bigg]\quad\text{for } k>N-2c. \tag{10}$$

By approximating the Toeplitz matrix $\mathbf{G}$ to a circulant matrix $\mathbf{G}_{\mathrm{c}}$ [22], the first column of $\mathbf{G}_{\mathrm{c}}$ can be denoted by $[g(0),g(T),\cdots,g(2cT),0,\cdots,0,g(-2cT),\cdots,g(-T)]^T$. Furthermore, we can obtain

$$\begin{aligned}\mathbf{G}_{\mathrm{r}}&\approx(\mathbf{I}_{N_r}\otimes\mathbf{G}_{\mathrm{c}})\in\mathbb{R}^{NN_r\times NN_r}\\&=\widetilde{\mathbf{G}}_{\mathrm{c}},\end{aligned} \tag{11}$$

where $\widetilde{\mathbf{G}}_{\mathrm{c}}=(\mathbf{I}_{N_r}\otimes\mathbf{G}_{\mathrm{c}})$.

Hence, using (9), (10) and (11), (8) is approximated to

$$\hat{\mathbf{s}}\approx\mathbf{H}_{\mathrm{s}}^H\left(\mathbf{H}_{\mathrm{s}}\mathbf{H}_{\mathrm{s}}^H+\sigma_0^2\widetilde{\mathbf{G}}_{\mathrm{c}}\right)^{-1}\mathbf{y}, \tag{12}$$

where

$$\mathbf{H}_{\mathrm{s}}=\begin{bmatrix}\hat{\mathbf{H}}_{1,1}&\cdots&\hat{\mathbf{H}}_{1,N_t}\\\vdots&\ddots&\vdots\\\hat{\mathbf{H}}_{N_r,1}&\cdots&\hat{\mathbf{H}}_{N_r,N_t}\end{bmatrix}\in\mathbb{C}^{NN_r\times NN_t}. \tag{13}$$

To reduce the band of active elements in $\mathbf{H}_{\mathrm{s}}\mathbf{H}_{\mathrm{s}}^H+\sigma_0^2\widetilde{\mathbf{G}}_{\mathrm{c}}$, we reorder the matrix to a banded matrix by using the reverse Cuthil-Mckee algorithm [23], where Figs. 1(a) and 1(b) show the before and after the matrix reorder, respectively. The complexity imposed by the reverse Cuthil-Mckee algorithm is given by $O(N_z+NN_r\log d)$ [24], where N_z is the number of non-zero elements in the matrix, and d is the average degree of the graph constructed in the algorithm. The reordered matrix $\mathbf{\Psi}\in\mathbb{C}^{NN_r\times NN_r}$ is denoted as $\mathbf{\Psi}=\mathbf{P}(\mathbf{H}_{\mathrm{s}}\mathbf{H}_{\mathrm{s}}^H+\sigma_0^2\widetilde{\mathbf{G}}_{\mathrm{c}})\mathbf{P}^T$, where $\mathbf{P}\in\mathbb{R}^{NN_r\times NN_r}$ is the permutation matrix computed by the reverse Cuthil-Mckee algorithm, which satisfies $\mathbf{P}\mathbf{P}^T=\mathbf{I}_{NN_r}$. Considering the Choleskey factorization of $\mathbf{\Psi}=\widetilde{\mathbf{L}}\widetilde{\mathbf{U}}$, where we have $\widetilde{\mathbf{L}}=\widetilde{\mathbf{U}}^H$, we can obtain

$$\begin{aligned}&\widetilde{\mathbf{L}}\widetilde{\mathbf{U}}=\mathbf{P}(\mathbf{H}_{\mathrm{s}}\mathbf{H}_{\mathrm{s}}^H+\sigma_0^2\widetilde{\mathbf{G}}_{\mathrm{c}})\mathbf{P}^T\\&\Leftrightarrow(\mathbf{H}_{\mathrm{s}}\mathbf{H}_{\mathrm{s}}^H+\sigma_0^2\widetilde{\mathbf{G}}_{\mathrm{c}})^{-1}=\mathbf{P}^T\widetilde{\mathbf{U}}^{-1}\widetilde{\mathbf{L}}^{-1}\mathbf{P}.\end{aligned} \tag{14}$$

Hence, (12) is rewritten to

$$\hat{\mathbf{s}}=\mathbf{H}_{\mathrm{s}}^H\mathbf{P}^T\overbrace{\underbrace{\widetilde{\mathbf{U}}^{-1}\underbrace{\widetilde{\mathbf{L}}^{-1}\underbrace{\mathbf{P}\mathbf{y}}_{\mathbf{s}'}}_{\mathbf{s}''}}}^{\mathbf{s}'''}. \tag{15}$$

The complexity of the Cholesky factorization $\mathbf{\Psi}=\widetilde{\mathbf{L}}\widetilde{\mathbf{U}}$ is $O(NN_rB_w^2)$, where B_w is the bandwidth of active elements in the matrix $\mathbf{\Psi}$, and the complexity of $\mathbf{s}'=\mathbf{P}\mathbf{y}$ is $O(NN_r)$. Considering the band structure of $\widetilde{\mathbf{L}}$, $\mathbf{s}''=\widetilde{\mathbf{L}}^{-1}\mathbf{s}'$ can be computed by the forward substitution algorithm for a banded matrix [24]. Similarly, $\mathbf{s}'''=\widetilde{\mathbf{U}}^{-1}\mathbf{s}''$ can be calculated by the backward substitution algorithm for a banded matrix [24]. Each complexity of the forward substitution algorithm and the backward substitution algorithm is $O(NN_rB_w)$. The complexity of $\hat{\mathbf{s}}=\mathbf{H}_{\mathrm{s}}^H\mathbf{P}^T\mathbf{s}'''$ is $O(NN_r+N_tN_rc)$. Hence, the total complexity for (15) is summarized as $O(N_r(NB_w^2+N_tc))$.

B. Achievable Information Rate

Let us define $\widetilde{\mathbf{W}}=\mathbf{H}_{\mathrm{s}}^H\mathbf{P}^T\widetilde{\mathbf{U}}^{-1}\widetilde{\mathbf{L}}^{-1}\mathbf{P}$, $\widetilde{\mathbf{H}}_{\mathrm{eff}}=\widetilde{\mathbf{W}}\mathbf{H}$, and $\widetilde{\boldsymbol{\eta}}_{\mathrm{eff}}=\widetilde{\mathbf{W}}\boldsymbol{\eta}$. Then, the mutual information $I(\mathbf{s};\hat{\mathbf{s}})$ between the received symbols $\hat{\mathbf{s}}$ and the transmit symbols $\mathbf{s}$ can be upper-bounded by

$$\begin{aligned}I(\mathbf{s};\hat{\mathbf{s}})=h_e(\hat{\mathbf{s}})-h_e(\hat{\mathbf{s}}|\mathbf{s})&\le\log_2\frac{(\pi e)^{NN_t}|\mathbb{E}[\hat{\mathbf{s}}\hat{\mathbf{s}}^H]|_{\det}}{(\pi e)^{NN_t}|\mathbb{E}[\widetilde{\boldsymbol{\eta}}_{\mathrm{eff}}\widetilde{\boldsymbol{\eta}}_{\mathrm{eff}}^H]|_{\det}}\\&=\log_2\left|\mathbf{I}+\frac{\sigma_s^2}{\sigma_0^2}\widetilde{\mathbf{G}}_{\mathrm{z}}^{-1}\widetilde{\mathbf{H}}_{\mathrm{eff}}\widetilde{\mathbf{H}}_{\mathrm{eff}}^H\right|_{\det},\end{aligned} \tag{16}$$

where the Hermitian matrix $\widetilde{\mathbf{G}}_{\mathrm{z}} = \widetilde{\mathbf{W}}\mathbf{G}_{\mathrm{r}}\widetilde{\mathbf{W}}^H \in \mathbb{C}^{NN_t \times NN_t}$ and the corresponding EVD is expressed as follows:

$$\widetilde{\mathbf{G}}_{\mathrm{z}} = \widetilde{\mathbf{V}}\widetilde{\mathbf{\Lambda}}_{\mathrm{z}}\widetilde{\mathbf{V}}^H, \tag{17}$$

where $\widetilde{\mathbf{V}} \in \mathbb{C}^{NN_t \times NN_t}$ is the unitary matrix and $\widetilde{\mathbf{\Lambda}}_{\mathrm{z}} \in \mathbb{R}^{NN_t \times NN_t}$ is a diagonal matrix. With (17), (16) is further simplified to

$$I(\mathbf{s};\hat{\mathbf{s}}) = \log_2 \left| \mathbf{I} + \frac{\sigma_s^2}{\sigma_0^2} \widetilde{\mathbf{H}}_{\mathrm{eff}}^H \widetilde{\mathbf{V}} \widetilde{\mathbf{\Lambda}}_{\mathrm{z}}^{-\frac{1}{2}} \widetilde{\mathbf{\Lambda}}_{\mathrm{z}}^{-\frac{1}{2}} \widetilde{\mathbf{V}}^H \widetilde{\mathbf{H}}_{\mathrm{eff}} \right|_{\mathrm{det}}, \tag{18}$$

where $\widetilde{\mathbf{D}}_{\mathrm{z}} = \widetilde{\mathbf{\Lambda}}_{\mathrm{z}}^{-\frac{1}{2}} \widetilde{\mathbf{V}}^H \widetilde{\mathbf{H}}_{\mathrm{eff}} \in \mathbb{C}^{NN_t \times NN_t}$. Then, the EVD of $\widetilde{\mathbf{D}}_{\mathrm{z}}^H \widetilde{\mathbf{D}}_{\mathrm{z}}$ is given by $\widetilde{\mathbf{D}}_{\mathrm{z}}^H \widetilde{\mathbf{D}}_{\mathrm{z}} = \widetilde{\mathbf{U}}_{\mathrm{z}} \widetilde{\mathbf{\Xi}} \widetilde{\mathbf{U}}_{\mathrm{z}}^H$, where $\widetilde{\mathbf{U}}_{\mathrm{z}} \in \mathbb{C}^{NN_t \times NN_t}$ is the unitary matrix, and $\widetilde{\mathbf{\Xi}} \in \mathbb{R}^{NN_t \times NN_t}$ is a diagonal matrix, having the NN_t descending-order eigenvalues $\widetilde{\xi}_0, \cdots, \widetilde{\xi}_{NN_t-1}$. Hence, (18) is modified to

$$I(\mathbf{s};\hat{\mathbf{s}}) = \log_2 \left| \mathbf{I} + \frac{\sigma_s^2}{\sigma_0^2} \widetilde{\mathbf{D}}_{\mathrm{z}}^H \widetilde{\mathbf{D}}_{\mathrm{z}} \right|_{\mathrm{det}} = \sum_{i=0}^{NN_t-1} \log_2 \left(1 + \frac{\sigma_s^2 \widetilde{\xi}_i}{\sigma_0^2} \right). \tag{19}$$

IV. Extension to MIMO-OTFS-FTN Signaling

Consider the two-dimensional information symbols in the DD-domain, which are transmitted from the v-th transmit antenna, are represented by $\widetilde{\mathbf{S}}_v \in \mathbb{C}^{\widetilde{M} \times \widetilde{N}}$, where $\widetilde{M}$ and $\widetilde{N}$ denote the number of subcarriers and that of time slots in each frame. Furthermore, the information symbols from N_t transmit antennas are defined by $\widetilde{\mathbf{s}} = [\widetilde{\mathbf{s}}_1^T, \cdots, \widetilde{\mathbf{s}}_{N_t}^T]^T \in \mathbb{C}^{\widetilde{M}\widetilde{N}N_t}$, where $\widetilde{\mathbf{s}}_v = \mathrm{vec}(\widetilde{\mathbf{S}}_v)$. The FTN sampling interval is $T = \alpha T_0 = \widetilde{T}/\widetilde{M}$, where $\widetilde{T} = 1/\Delta f$ and Δf is subcarrier spacing.

In order to convert the symbols modulated in the DD-domain to the transmitted symbols in the time-frequency domain, the inverse symplectic fast Fourier transform (ISFFT) is carried out, which corresponds to the $\widetilde{M}$-point FFT for the columns and the $\widetilde{N}$-point IFFT for the rows as follows: $\widetilde{\mathbf{X}}_v = \mathbf{F}_{\widetilde{M}}^H \left(\mathbf{F}_{\widetilde{M}} \widetilde{\mathbf{S}}_v \mathbf{F}_{\widetilde{N}}^H \right) \in \mathbb{C}^{\widetilde{M} \times \widetilde{N}}$ [25], where $\widetilde{\mathbf{X}}_v$ denotes the TD symbols of the v-th transmit antenna. Furthermore, the column-wise vectorization of $\widetilde{\mathbf{X}}_v$ is represented by $\widetilde{\mathbf{x}}_v = \mathrm{vec}(\widetilde{\mathbf{X}}_v) = \left(\mathbf{F}_{\widetilde{N}}^H \otimes \mathbf{I}_{\widetilde{M}} \right) \widetilde{\mathbf{s}}_v \in \mathbb{C}^{\widetilde{M}\widetilde{N}}$.

Owing to the channel's sparsity in the DD domain, the time-varying channel's response between the u-th receiver and the v-th transmitter is formulated by: $h_{uv}(\tau,\nu) = \sum_{i=0}^{L-1} h_{uv,i} \delta(\tau - \tau_{uv,i}) \delta(\nu - \nu_{uv,i})$ [26], where $\delta(\cdot)$ is Dirac's delta function. Furthermore, $\tau_{uv,i}$ and $\nu_{uv,i}$ are the delay and the Doppler shift of the i-th path between the u-th receiver and the v-th transmitter, which are denoted by $\tau_{uv,i} = \widetilde{l}_{uv,i}/\widetilde{M}\Delta f$ and $\nu_{uv,i} = (\widetilde{k}_{uv,i} + \widetilde{\kappa}_{uv,i})/\widetilde{N}\widetilde{T}$, respectively. Note that $\widetilde{l}_{uv,i}$ and $\widetilde{k}_{uv,i}$ are the integer parameters, corresponding to the delay and Doppler shift, and $\widetilde{\kappa}_{uv,i}$ represents the fractional Doppler shift for $-1/2 < \widetilde{\kappa}_{uv,i} \leq 1/2$. We assume that the channel's maximum delay $\tau_{\max}$ and maximum Doppler shift $\nu_{\max}$ satisfy $\tau_{\max} \leq (2c-1)\widetilde{T}/\widetilde{M}$ and $|\nu_{\max}| \leq \Delta f/2$, respectively. Furthermore, $\widetilde{l}_{\max}$ and $\widetilde{k}_{\max}$ correspond to $\tau_{\max}$ and $\nu_{\max}$.

Under the assumption of $2c$-length CP symbols in each block, the channel matrix between the u-th transmit and the v-th receive antennas after the removal of the CP is represented by $\mathbf{H}_{u,v}^{\mathrm{otfs}} = \mathbf{R}_{\mathrm{cp}} \widetilde{\mathbf{H}}_{u,v}^{\mathrm{otfs}} \mathbf{A}_{\mathrm{cp}}$, where the effective channel matrix $\widetilde{\mathbf{H}}_{u,v}^{\mathrm{otfs}}$ includes the effects of FTN sampling, and the kth-row and mth-column entry of $\widetilde{\mathbf{H}}_{u,v}^{\mathrm{otfs}}$ is given by $\widetilde{\mathbf{H}}_{u,v}^{\mathrm{otfs}}[k,m] = \sum_{i=0}^{L-1} h_{uv,i} e^{j2\pi \frac{(\widetilde{k}_{uv,i} + \widetilde{\kappa}_{uv,i})(k - \widetilde{l}_{uv,i})}{\widetilde{M}\widetilde{N}}} g\left(kT - \left(m + \widetilde{l}_{uv,i} \right) T \right)$ [20]. Similar to (9) and (10), we carry out the sparse matrix approximation of $\hat{\mathbf{H}}_{\mathrm{u,v}}^{\mathrm{otfs}} \in \mathbb{C}^{\widetilde{M}\widetilde{N} \times \widetilde{M}\widetilde{N}} \approx \mathbf{H}_{u,v}^{\mathrm{otfs}}$, whose k-th row is given by

$$\Bigg[\underbrace{0, \ldots, 0}_{k-1}, \sum_{i=0}^{L-1} h_{uv,i} e^{j2\pi \frac{\left(\widetilde{k}_{uv,i} + \widetilde{\kappa}_{uv,i}\right)(k+c-\widetilde{l}_{uv,i})}{\widetilde{M}\widetilde{N}}} g((-c + \widetilde{l}_{uv,i})T), \ldots, \sum_{i=0}^{L-1} h_{uv,i} e^{j2\pi \frac{\left(\widetilde{k}_{uv,i} + \widetilde{\kappa}_{uv,i}\right)(k+c-\widetilde{l}_{uv,i})}{\widetilde{M}\widetilde{N}}} g((c + \widetilde{l}_{uv,i})T), \underbrace{0, \ldots, 0}_{\widetilde{M}\widetilde{N} - 2c - k} \Bigg] \text{ for } k \leq \widetilde{M}\widetilde{N} - 2c,$$

and

$$\Bigg[\sum_{i=0}^{L-1} h_{uv,i} e^{j2\pi \frac{\left(\widetilde{k}_{uv,i} + \widetilde{\kappa}_{uv,i}\right)(k+c-\widetilde{l}_{uv,i})}{\widetilde{M}\widetilde{N}}} \times g((\widetilde{M}\widetilde{N} - c - k + \widetilde{l}_{uv,i} + 1)T), \ldots, \sum_{i=0}^{L-1} h_{uv,i} e^{j2\pi \frac{\left(\widetilde{k}_{uv,i} + \widetilde{\kappa}_{uv,i}\right)(k+c-\widetilde{l}_{uv,i})}{\widetilde{M}\widetilde{N}}} g((c + \widetilde{l}_{uv,i})T), \underbrace{0, \ldots, 0}_{\widetilde{M}\widetilde{N} - 2c - 1}, \sum_{i=0}^{L-1} h_{uv,i} e^{j2\pi \frac{\left(\widetilde{k}_{uv,i} + \widetilde{\kappa}_{uv,i}\right)(k+c-\widetilde{l}_{uv,i})}{\widetilde{M}\widetilde{N}}} g((-c + \widetilde{l}_{uv,i})T), \ldots, \sum_{i=0}^{L-1} h_{uv,i} e^{j2\pi \frac{\left(\widetilde{k}_{uv,i} + \widetilde{\kappa}_{uv,i}\right)(k+c-\widetilde{l}_{uv,i})}{\widetilde{M}\widetilde{N}}} g((\widetilde{M}\widetilde{N} - c - k + \widetilde{l}_{uv,i})T) \Bigg]. \quad \text{for } k > \widetilde{M}\widetilde{N} - 2c$$

Hence, the approximated received signal is expressed as $\widetilde{\mathbf{y}} \approx \widetilde{\mathbf{H}}\widetilde{\mathbf{Q}}\widetilde{\mathbf{s}} + \widetilde{\boldsymbol{\eta}} \in \mathbb{C}^{\widetilde{M}\widetilde{N}N_r}$, where $\widetilde{\mathbf{Q}} = \mathbf{I}_{N_t} \otimes \left(\mathbf{F}_{\widetilde{N}}^H \otimes \mathbf{I}_{\widetilde{M}} \right)$ and

$$\widetilde{\mathbf{H}} = \begin{bmatrix} \hat{\mathbf{H}}_{1,1}^{\mathrm{otfs}} & \cdots & \hat{\mathbf{H}}_{1,\mathrm{N_t}}^{\mathrm{otfs}} \\ \vdots & \ddots & \vdots \\ \hat{\mathbf{H}}_{\mathrm{N_r},1}^{\mathrm{otfs}} & \cdots & \hat{\mathbf{H}}_{\mathrm{N_r},\mathrm{N_t}}^{\mathrm{otfs}} \end{bmatrix} \in \mathbb{C}^{\widetilde{M}\widetilde{N}N_r \times \widetilde{M}\widetilde{N}N_t}. \tag{20}$$

Then, we arrive at

$$\hat{\mathbf{s}}_{\mathrm{otfs}} \approx \widetilde{\mathbf{Q}}^H \widetilde{\mathbf{H}}^H \left(\widetilde{\mathbf{H}}\widetilde{\mathbf{H}}^H + \sigma_0^2 \widetilde{\mathbf{G}}_{\mathrm{c}}^{\mathrm{otfs}} \right)^{-1} \widetilde{\mathbf{y}}, \tag{21}$$

where $\widetilde{\mathbf{G}}_{\mathrm{c}}^{\mathrm{otfs}} = (\mathbf{I}_{N_r} \otimes \mathbf{G}_{\mathrm{c}}^{\mathrm{otfs}})$. Similar to an approximation of (11), $\mathbf{G}_{\mathrm{c}}^{\mathrm{otfs}} \in \mathbb{C}^{\widetilde{M}\widetilde{N} \times \widetilde{M}\widetilde{N}}$ is given by the circulant matrix, whose first column is $[g(0), g(T), \cdots, g(2cT), 0, \cdots, 0, g(-2cT), \cdots, g(-T)]^T$. Observe that $\widetilde{\mathbf{H}}\widetilde{\mathbf{H}}^H + \sigma_0^2 \widetilde{\mathbf{G}}_{\mathrm{c}}^{\mathrm{otfs}}$ in (21) has the same sparse structure as that considered in Fig. 1(a). Hence, the reduced-complexity LMMSE detector in Section III is readily applicable to the MIMO-OTFS-FTN signaling system.

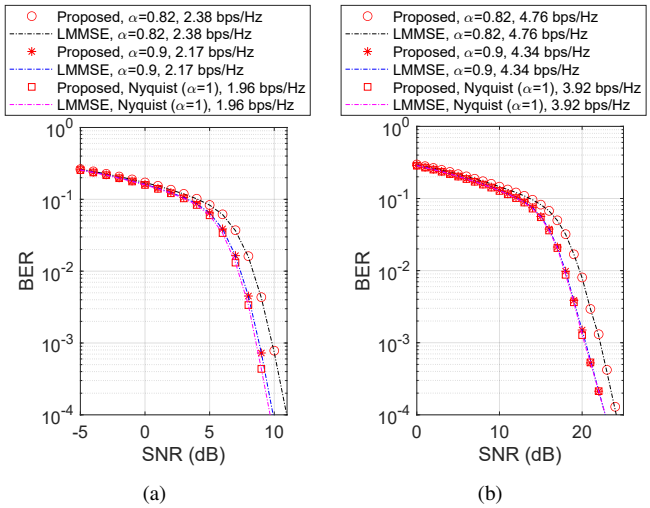

(a) (b)

Fig. 2. BER performance of the proposed detection scheme for the MIMO-FTN signaling scheme in the doubly-selective fading channel, compared with the full-complexity LMMSE bound: (a) QPSK and (b) 16QAM.

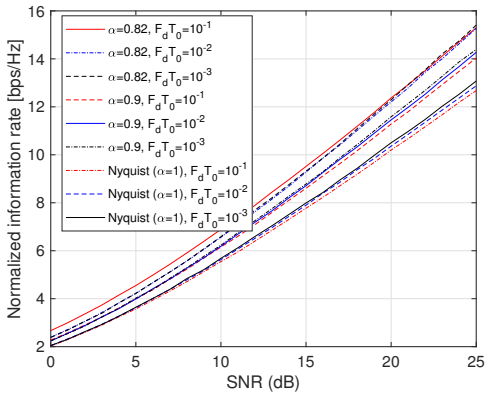

Fig. 3. Achievable information rate of the proposed MIMO-FTN signaling scheme in the doubly fading channels for different packing ratios.

V. Performance Results

In this section, we provide our performance results to analyze the proposed MIMO-FTN and MIMO-OTFS-FTN signaling schemes in the doubly selective fading channels. We assume that each channel coefficient $h_{uv,i}$ is independently generated according to the complex-valued Gaussian distribution $h_{uv,i} \sim \mathcal{CN}(0, 1/L)$ per frame. Moreover, the roll-off factor is set as $\beta = 0.25$ unless otherwise stated. In order to achieve a near-capacity BER performance, a 3/4-rate low-density parity check (LDPC) coding scheme with a maximum number of iterations of 50 is used. We define the transmission rate as $R_{\rm t} = \frac{3}{4}\frac{1}{2W(1+\beta)}\frac{1}{(N+2c)\alpha T_0}\sum_{n=0}^{NN_t-1} b_n [\text{bps/Hz}]$, where b_n is the information bits mapped onto the n-th symbol, and 3/4 denotes the code rate.

Figs. 2(a) and 2(b) show the achievable BERs of the proposed low-complexity detection scheme for the MIMO-FTN signaling scheme in the doubly-selective fading channel, where QPSK and 16-QAM are employed, respectively. We consider the 2×2 MIMO system with the system parameters of $(N, L, c, F_dT_0) = (264, 10, 30, 0.01)$. The channel coefficients are generated based on Jakes fading model with 20 scatterers. Observe in Fig. 2 that the proposed scheme achieves the BER performance close to that of the full-complexity bound.

Furthermore, Fig. 3 shows the achievable information rate of the proposed scheme for the different normalized Doppler shifts of $F_dT_0 = 0.1$, 0.01, and 0.001. The other parameters are given by $(N_t, N_r, N, L, c) = (2, 2, 512, 10, 30)$. Observe in Fig. 3 that the proposed scheme tends to achieve the highest achievable information rate.

Figs. 4(a) and 4(b) show the BER performance of the proposed reduced-complexity detection scheme for the MIMO-OTFS-FTN signaling scheme in the doubly selective fading channel, which is compared with the full-complexity LMMSE bound, where QPSK and 16-QAM are employed, respectively. The system parameters are set as $(N_t, N_r, \widetilde{M}, \widetilde{N}, L, c, \widetilde{l}_{\max}, \widetilde{k}_{\max}) = (2, 2, 128, 6, 8, 30, 8, 2)$. Observe in Figs. 4(a) and 4(b) that the proposed reduced-complexity detection scheme achieves the performance close to the full-complexity LMMSE bound while achieving significantly low complexity. Furthermore, for $\alpha = 0.9$, the proposed scheme achieves a comparable BER performance to that of the Nyquist-based counterpart, which corresponds to the conventional MIMO-OTFS scheme while accomplishing a higher transmission rate.

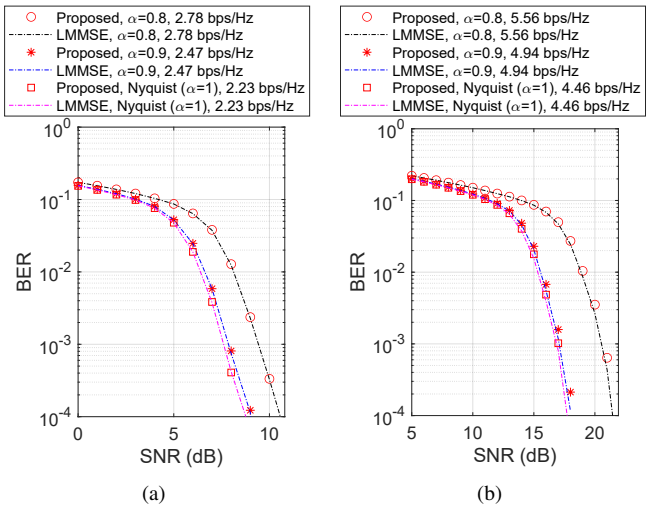

(a) (b)

Fig. 4. BER performance of the proposed detection scheme for the MIMO-OTFS-FTN signaling scheme: (a) QPSK and (b) 16QAM. The full-complexity LMMSE bound is plotted as the benchmark.

In Fig. 5, we investigated the achievable BERs of the proposed scheme for the packing ratio of $\alpha = 0.85$ and 0.9. Here, the EVD-precoded scheme without power allocation [20] is considered as the benchmark, which requires CSI at the transmitter and the receiver. The system parameters are given by $(N_t, N_r, \widetilde{M}, \widetilde{N}, L, c, \widetilde{l}_{\max}, \widetilde{k}_{\max}) = (2, 2, 128, 6, 6, 30, 6, 2)$, while bit-loading [7, 8] is used to achieve the target transmission rate. In Fig. 5, it is found that the proposed scheme out-

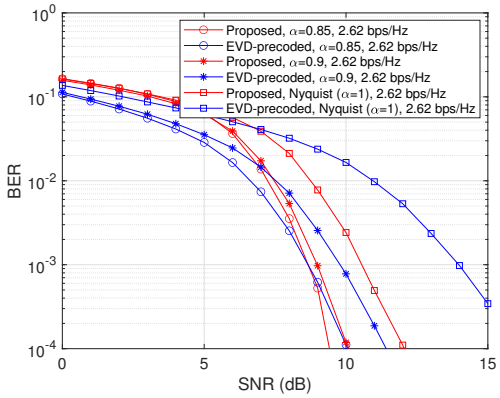

Fig. 5. BER performance of the proposed reduced-complexity detection for the MIMO-OTFS-FTN signaling scheme, which is compared with the EVD-precoded detector [20].

performs the conventional Nyquist-based MIMO-OTFS counterpart under the same transmission rate, which is achieved owing to the exploitation of excess bandwidth. Note that the detection complexity imposed by the EVD-based scheme is $O(N_t^3 \widetilde{M}^3 \widetilde{N}^3)$, which is significantly higher than that of the proposed scheme.

VI. Conclusions

In this paper, we proposed the reduced-complexity detection algorithm for the MIMO-FTN and MIMO-OTFS-FTN signaling schemes for the doubly selective fading channels, which relies on the sparsity approximation as well as LMMSE-based linear detection. Our performance results demonstrated that the proposed scheme exhibited a higher information rate than the conventional Nyquist-based counterpart using the same RRC shaping filter.

Acknowledgement

This work was supported in part by the JST SPRING (Grant JPMJSP2108), in part by JST FOREST (Grant JPMJFR2127), in part by JST ASPIRE (Grant JPMJAP2345), and in part by the JSPS KAKENHI (Grants 22H01481, 23K22752).

References

[1] T. Ishihara, S. Sugiura, and L. Hanzo, "The evolution of faster-than-Nyquist signaling," *IEEE Access*, vol. 9, pp. 86 535–86 564, Jun. 2021.

[2] A. Prlja and J. B. Anderson, "Reduced-complexity receivers for strongly narrowband intersymbol interference introduced by faster-than-Nyquist signaling," *IEEE Trans. Commun.*, vol. 60, no. 9, pp. 2591–2601, Sep. 2012.

[3] S. Sugiura, "Frequency-domain equalization of faster-than-Nyquist signaling," *IEEE Wireless Commun. Lett.*, vol. 2, no. 5, pp. 555–558, Oct. 2013.

[4] S. Sugiura and L. Hanzo, "Frequency-domain-equalization-aided iterative detection of faster-than-Nyquist signaling," *IEEE Trans. Veh. Technol.*, vol. 64, no. 5, pp. 2122–2128, May 2015.

[5] Y. Ma, N. Wu, J. A. Zhang, B. Li, and L. Hanzo, "Generalized approximate message passing equalization for multi-carrier faster-than-Nyquist signaling," *IEEE Trans. Veh. Technol.*, vol. 71, no. 3, pp. 3309–3314, Mar. 2021.

[6] Y. J. Daniel Kim, "Properties of faster-than-Nyquist channel matrices and folded-spectrum, and their applications," in *Proc. IEEE WCNC*, Apr. 2016, pp. 1–7.

[7] T. Ishihara and S. Sugiura, "SVD-precoded faster-than-Nyquist signaling with optimal and truncated power allocation," *IEEE Trans. Wireless Commun.*, vol. 18, no. 12, pp. 5909–5923, Dec. 2019.

[8] ——, "Eigendecomposition-precoded faster-than-Nyquist signaling with optimal power allocation in frequency-selective fading channels," *IEEE Trans. Wireless Commun.*, vol. 21, no. 3, pp. 1681–1693, Mar. 2022.

[9] ——, "Reduced-complexity FFT-spread multicarrier faster-than-Nyquist signaling in frequency-selective fading channel," *IEEE Open J. Commun. Soc.*, vol. 3, pp. 530–542, Mar. 2022.

[10] N. Wu, W. Yuan, H. Wang, Q. Shi, and J. Kuang, "Frequency-domain iterative message passing receiver for faster-than-Nyquist signaling in doubly selective channels," *IEEE Wireless Commun. Lett.*, vol. 5, no. 6, pp. 584–587, Dec. 2016.

[11] J. Zhou, T. Ishihara, and S. Sugiura, "Precoded faster-than-Nyquist signaling for doubly selective underwater acoustic communication channel," *IEEE Wireless Commun. Lett.*, vol. 11, no. 10, pp. 2041–2045, Oct. 2022.

[12] T. Ishihara and S. Sugiura, "Differential multi-carrier faster-than-Nyquist signaling in doubly selective fading channel," *IEEE Trans. Veh. Technol.*, vol. 73, no. 1, pp. 1424–1429, Jan. 2024.

[13] F. Rusek, "A first encounter with faster-than-Nyquist signaling on the MIMO channel," in *2007 IEEE Wireless Communications and Networking Conference*, Mar. 2007, pp. 1093–1097.

[14] M. Yuhas, Y. Feng, and J. Bajcsy, "On the capacity of faster-than-Nyquist MIMO transmission with CSI at the receiver," in *2015 IEEE Globecom Workshops (GC Wkshps)*, Dec. 2015, pp. 1–6.

[15] Z. Zhang, M. Yuksel, and H. Yanikomeroglu, "Faster-than-Nyquist signaling for MIMO communications," *IEEE Trans. Wireless Commun.*, vol. 22, no. 4, pp. 2379–2392, Apr. 2023.

[16] S. Wen, G. Liu, F. Xu, L. Zhang, C. Liu, and M. A. Imran, "Ergodic capacity of MIMO faster-than-Nyquist transmission over triply-selective Rayleigh fading channels," *IEEE Trans. Commun.*, vol. 70, no. 8, pp. 5046–5058, Aug. 2022.

[17] M. Guo, Y. Qiao, J. Zhou, X. Tang, J. Qi, S. Liu, X. Xu, and Y. Lu, "ICI cancellation based on MIMO decoding for FTN Non-Orthogonal FDM systems," *J. Lightw. Technol.*, vol. 37, no. 3, pp. 1045–1055, Feb. 2019.

[18] H.-T. Chiu, S. Saito, H. Suganuma, K. Kuriyama, K. Tanaka, H. Hasegawa, T. Miyagi, T. Onizawa, and F. Maehara, "Performance evaluation of MIMO-FTN signaling under multipath fading channels," *IEEE Access*, vol. 11, pp. 89 383–89 392, 2023.

[19] Y. Zhang, B. Ning, W. Ni, J. Wang, W. Tang, and D. Niyato, "Exploiting faster-than-Nyquist signaling for MIMO covert communications: A low-complexity design," *IEEE Trans. Veh. Technol.*, vol. 73, no. 5, pp. 7322–7327, May 2024.

[20] Z. Hong, S. Sugiura, C. Xu, and L. Hanzo, "Precoded faster-than-Nyquist signaling using optimal power allocation for OTFS," *IEEE Wireless Commun. Lett.*, vol. 14, no. 1, pp. 173–177, Jan. 2025.

[21] X. Yang, B. Zhang, M. Zhou, and M. Gao, "Integrated sensing and communications waveform design for OTFS and FTN fusion," *IEEE Signal Process. Lett.*, vol. 31, pp. 2870–2874, Oct. 2024.

[22] R. M. Gray *et al.*, "Toeplitz and circulant matrices: A review," *Foundations and Trends® in Communications and Information Theory*, vol. 2, no. 3, pp. 155–239, 2006.

[23] P. Singh, S. Tiwari, and R. Budhiraja, "Low-complexity LMMSE receiver design for practical-pulse-shaped MIMO-OTFS systems," *IEEE Trans. Commun.*, vol. 70, no. 12, pp. 8383–8399, Dec. 2022.

[24] G. H. Golub and C. F. Van Loan, *Matrix computations*. JHU press, 2013.

[25] C. Xu, L. Xiang, S. Sugiura, R. G. Maunder, L.-L. Yang, D. Niyato, G. Y. Li, R. Schober, and L. Hanzo, "Noncoherent orthogonal time frequency space modulation," *IEEE Trans. Wireless Commun.*, vol. 23, no. 8, pp. 10 072–10 090, Aug. 2024.

[26] R. Hadani, S. Rakib, M. Tsatsanis, A. Monk, A. J. Goldsmith, A. F. Molisch, and R. Calderbank, "Orthogonal time frequency space modulation," in *2017 IEEE Wireless Communications and Networking Conference (WCNC)*, May 2017, pp. 1–6.